Energy 187 (2019) 115938

Contents lists available at ScienceDirect

Energy

journal homepage: www.elsevier.com/locate/energy

Global estimations of wind energy potential considering seasonal air density changes

Alain Ulazia [a, *], Jon Sáenz [b, c], Gabriel Ibarra-Berastegi [c, d], Santos J. González-Rojí [e, f], Sheila Carreno-Madinabeitia [g]

[a] Department of NE and Fluid Mechanics, University of the Basque Country (UPV/EHU), Otaola 29, 20600, Eibar, Spain
[b] Department of Applied Physics II, University of the Basque Country (UPV/EHU), B. Sarriena S/n, 48940, Leioa, Spain
[c] Joint Research Unit (UPV/EHU-IEO) Plentziako Itsas Estazioa, University of the Basque Country (UPV/EHU), Areatza Hiribidea 47, 48620, Plentzia, Spain
[d] Department of NE and Fluid Mechanics, University of the Basque Country (UPV/EHU), Alda, Urkijo, 48013, Bilbao, Spain
[e] Now at: Oeschger Centre for Climate Change Research and Climate and Environmental Physics, University of Bern, Bern, Switzerland
[f] Climate and Environmental Physics, University of Bern, Bern, Switzerland
[g] Tecnalia, Parque Tecnológico de Alava, Vitoria-Gasteiz, Spain

ARTICLE INFO

Article history:
Received 7 May 2019
Received in revised form
29 July 2019
Accepted 11 August 2019
Available online 14 August 2019

Keywords:
Wind energy potential
Air density
ERA5
Fluid mechanics

ABSTRACT

The literature typically considers constant annual average air density when computing the wind energy potential of a given location. In this work, the recent reanalysis ERA5 is used to obtain global seasonal estimates of wind energy production that include seasonally varying air density. Thus, errors due to the use of a constant air density are quantified. First, seasonal air density changes are studied at the global scale. Then, wind power density errors due to seasonal air density changes are computed. Finally, winter and summer energy production errors due to neglecting the changes in air density are computed by implementing the power curve of the National Renewable Energy Laboratorys 5 MW turbine. Results show relevant deviations for three variables (air density, wind power density, and energy production), mainly in the middle-high latitudes (Hudson Bay, Siberia, Patagonia, Australia, etc.). Locations with variations from −6% to 6% are identified from summers to winters in the Northern Hemisphere. Additionally, simulations with the aeroelastic code FAST for the studied turbine show that instantaneous power production can be affected by greater than 20% below the rated wind speed if a day with realistically high or low air density values is compared for the same turbulent wind speed.

1. Introduction

Wind energy potential estimation is often based mainly on wind speed and the power curve of the turbine, and only marginally on the temporal and spatial variations in air density. Vertical changes in air density are normally taken into account. The annual average air density of the site is considered as a function of height when applying well-known models such as the standard atmospheric profile to obtain the mean pressure and temperature at that height and, as a result, the constant air density for that site. This may involve a complete redesign of the blade for wind turbines located at high altitudes and permanent functioning with air densities lower than the standard sea-level value [1,2].

Thus, air density is usually considered as constant during the year, with standard value ρ_0 being equal to 1.225 kg/m^3 (at sea level, 0 m.a.s.l., 15°C) as the reference for middle latitudes near the sea (see Table 1 for a list of important nomenclature). The use of constant air density is common for different types of estimation methods, namely.

- at specific locations using anemometers [3–5], and
- in certain geographical regions for estimation of spatially distributed wind energy using mesoscale models, remote sensing data, or reanalysis [6–17].

This is logical since the most common method for the estimation of Annual Energy Production (AEP) does not use air density: the Weibull distribution is fitted on the wind speed data of the location to be implemented on the turbine's power curve. Only the

* Corresponding author.
E-mail addresses: alain.ulazia@ehu.eus (A. Ulazia), jon.saenz@ehu.eus (J. Sáenz), gabriel.ibarra@ehu.eus (G. Ibarra-Berastegi), santosjose.gonzalez@ehu.eus (S.J. González-Rojí), sheila.carreno@tecnalia.com (S. Carreno-Madinabeitia).

https://doi.org/10.1016/j.energy.2019.115938

Table 1
Important nomenclature.

WRF	Weather Research and Forecasting Model
ECMWF	European Centre for Medium-Range Weather Forecasts
m.a.s.l	meters above sea level
p	Surface pressure
q	Specific humidity
e	Partial pressure of water vapour
T	Temperature
T_v	Virtual temperature
CF	Capacity Factor
WPD	Wind Power Density
ΔWPD	Relative change in Wind Power Density (in percent)
U	Wind speed
D	Wind turbine diameter
U_n	Normalized wind speed
ρ	Air density
ρ_0	Standard air density (1.225 kg/m^3)
$\overline{\rho_a}$	Local long-term mean air density
$\Delta\rho$	Change in air density (in percent)
P_R	Rated power of the wind turbine
$maxPR$	Maximum power ratio
AEP	Annual Energy Production
SEP	Seasonal Energy Production
ΔSEP	Change in SEP (in percent)

contribution of wind speed is considered, because the power curve is often provided for standard air density and is not corrected for the air density of the location.

However, the changes imposed by air density variations in wind potential are important globally, as will be shown by this study. This paper presents investigations of the impact of air density changes both onshore and Offshore which is possible due to the availability of global wind, surface pressure, temperature, and moisture data from the ERA5 new global reanalysis. The world's first floating wind farm, Statoil's HyWind Scotland pilot park, is already functional [18]. Such floating wind farms are expanding the available area compared to the limited sites offered by established turbines [19], and thus, are viewed as an interesting option by many countries [20]. Thus, a more realistic evaluation of global wind potential, currently possible with globally available meteorological data, is important, both for onshore and offshore places.

As a paradigmatic example, Farkas et al. [21] analysed the temporal variations in air density at a specific location in Hungary using neural networks, and proposed a correction to the power curve for a given wind turbine. The air density oscillates around the mean value, with variations reaching approximately 15%. As wind power is proportional to air density, this value clearly poses a significant deviation. Another such significant example was provided by Collins et al. [22] who showed that, for the same wind speed, the difference between power production on a hot day and power production on a cold day can be of the order of 10% for medium wind speeds. As another exceptional example, advances have been made towards incorporating air density and in the estimation of effective wind speed (normalized in technical terms) to consider the contribution of the real time-varying air density [23]. The Weibull distribution was fitted over this new wind speed time series and it was implemented in the power curve. However, the study was conducted at a punctual location.

The essential hypothesis of this normalization method for wind speed in order to accommodate the changes in air density can be formulated as follows.

1. Instead of the usual hypothesis, *the power production of the turbine is the same for the same wind speeds*, and
2. The hypothesis introduces air density in the wind power density (WPD) by assuming that *the power production of the turbine is the same for constant WPD.*

This methodology begins by defining *WPD*, the kinetic power of wind per unit area, by including both air density (ρ) and wind speed magnitude U in its definition, as below.

$$WPD = \frac{1}{2}\rho U^3 \tag{1}$$

If the constant and real air densities are ρ_0 and ρ respectively, and U and U_n denote the real and normalized wind speeds, the hypothesis establishes that the same amount of power is produced as long as WPD remains unchanged.

$$WPD_0 = WPD \Rightarrow \frac{1}{2}\rho U^3 = \frac{1}{2}\rho_0 U_n^3 \tag{2}$$

Thus, the following expression for the normalized wind speed is derived from the above equation.

$$U_n = \left(\frac{\rho}{\rho_0}\right)^{1/3} U. \tag{3}$$

This normalized wind magnitude can be implemented in the standard power curve designed for constant air density ρ_0 since the changes in wind potential due to the changes in wind density have already been included in the definition of the normalized wind magnitude U_n. The exponent of the normalization of the air density ratio is 1 /3 in this methodology. To adapt the power curve of the turbine to the air density of the location, Svenningsen proposed a new method which was adopted by WindPRO [24]. The exponent of normalization is not a constant of value 1 /3 for all wind speeds; it is redefined for different wind speed intervals. However, in this study, instead of adapting the power curve, we obtained the normalized wind speed using Eq. (3) and implemented it in the standard power curve of the selected turbine for each grid point of ERA5 ($0.25^\circ \times 0.25^\circ$) globally.

Here, we used a publicly available global reanalysis produced by ECMWF of high spatial resolution, but previously, temperature and pressure data from a mesoscale model have also been used for an offshore turbine to calculate the air density over Japanese waters [25]. The corresponding mesoscale model is a version of RAMS (year 2014), and a similar normalization of wind speed by means of air density is used to estimate wind power. However, the changes in seasonal wind power due to air density were not implemented in the power curve of that turbine (MWT-92/2.4, hub height: 70 m, Mitsubishi Heavy Industry). In our case, we chose a higher hub height of 90 m and a turbine of 5 MW for implementation in offshore or onshore wind farms (see Section 2.2.2 for details).

The objective of this paper is to study the global structure of seasonal air density changes and the manner in which they affect the wind energy potential worldwide, and to compare these results with the annual average corresponding to every grid point. These estimations of changes induced by air density variations are then applied to the Seasonal Energy Production (SEP) of the turbine installed at that location. In this study, we extended the results of Eurek et al. [26], who already considered the impact of density changes due to height, in the estimation of wind energy. However, we were not limited to changes due to different surface heights. We extend these results by taking into account the seasonal changes in air density. They can be due to temperature or surface pressure systems which change according to the seasonal evolution of global atmospheric circulation, including Hadley cells, as well as the seasonal distribution of extratropical pressure systems [27,28].

These seasonal changes due to air density in wind energy potential have been studied previously by the authors in the output files obtained from an integration with the Weather Research and Forecasting Model (WRF) model with 3DVAR data assimilation in regional resource assessment studies around the Iberian Peninsula. Here, the air density as well as wind speed were considered [29,30]. However, the current paper extends those previous findings to the global scale by using a recent high-quality global dataset.

Recently, Floors et al. [31] have published a work on air density effects for wind energy using ERA5, but for the influence of hub height in the air density correction. They emphasize like us that the effect of air density has been poorly studied in the literature, and propose and validate a new correction model for air density to be implemented in the well-known software WAsP. However, these corrections are for a referential air density value at the given location, which is used to select the corresponding adapted power curve. This referential value is constant and is based on the annual average, so it does not consider the seasonal or daily variations as in our work.

In this sense, this study is pioneering because it offers global maps to the wind industry developers in order to identify, in a prediagnosis stage, world regions with important seasonal wind energy variations due to air density changes. The fact that the spatial autocorrelation of temperature and pressure anomalies (the two factors which affect the most density changes) is well known [32–34]. These high spatial autocorrelations support the use of this global reanalysis for a first order estimate of the worldwide relevance of the phenomena. The resolution used in this paper, however, is relatively coarse and, for the deployment of new wind farms, a more detailed analysis would be needed at the local scale.

The main objective of this paper is to extend previous results along different lines. First, the impact of density in the evaluation of wind energy resources is extended to include the seasonal variability. Second, the results are estimated worlwide, so that a first order estimate of this effect is presented to the reader (Sections 3.1 to 3.3). Next, the impact of the efect on the real energy that can be produced at different wind regimes are also estimated using a FAST-based simulation (Section 3.4). Finally, the major players in the studied effect (first, temperature, second pressure, last, moisture) are clearly identified in the discussion (Section 4). This is particularly relevant for those cases in which researchers might have limited access to data.

The remainder of this paper is structured as follows. Section 2 describes the ERA5 reanalysis and its recent validations in the literature. Section 3 presents the main results of the paper and the global maps. Section 4 discusses the results and Section 5 concludes the paper and describes the scope for future studies.

2. Data and methodology

2.1. Data

2.1.1. Reanalysis ERA5

ERA5 is a recent reanalysis [35] developed at the European Centre for Medium-Range Weather Forecasts (ECMWF) (https://www.ecmwf.int/) and freely available through the Copernicus Climate Data Store (https://cds.climate.copernicus.eu/).

The ERA5 HRES atmospheric data are distributed at a resolution of 31 km and 0.28°. Among other variables, this reanalysis provides hourly values of the following variables of interest for this study: surface level pressure, relative humidity, temperature, and wind values at 10 and 100 m above ground level. The wind values are expressed as the zonal (U_{10} and U_{100}) and meridional (V_{10} and V_{100}) components of the wind vector. Before ERA5 was available, the authors conducted several wind energy studies using their own integrations obtained with the WRF meteorological model's outputs with data assimilation [29,30] nested into the ERA-Interim reanalysis [36], the previous ECMWF product with coarser resolution and data availability at 6 h steps. However, ERA5 is now readily available and provides a space and time resolution sufficient for wind energy studies ranging from the mesoscale to the global scale. At these scales, ERA5 negates the lengthy process of running specific integrations of meteorological models as in the WRF model. Accordingly, the authors successfully used ERA5 for several purposes such as studying the impact of air density changes on wind power in Scotland [37] and the identification of defective anemometers at a wind farm [38]. The potential of ERA5 for wind energy studies has been recently highlighted in the literature [39], and its use is quickly spreading to different areas in this field. ERA5 wind data have been used to assess wind energy potential in Latvia [40] and Africa [41], and as a reference to evaluate the performance of other high-resolution analyses for evaluating wind energy in Central Europe [42]. Other researchers have used ERA5 for different aspects of wind power such as developing energy lines for Europe [43] and analysing the impact of gravity waves on wind production [44]. ERA5 can also provide the wind field at different heights at the same space and time resolution, thus allowing the estimation of airborne wind energy potential [45]. Moreover, economic aspects of wind energy in Germany have been estimated using ERA5 [46]. Thus, since its recent release in 2016, ERA5 has become a reliable reference and an operative tool to address challenges which, as commented above, extend to a great number of aspects regarding wind energy studies. The next reanalysis, ERA6, is planned for approximately 2020 with even finer resolution (https://confluence.ecmwf.int/display/CKB/What+is+ERA5). The complete details of ERA5 reanalysis can be found at the ECMWF website (https://confluence.ecmwf.int/display/CKB/ERA5+data+documentation).

2.1.2. NRELs 5 MW turbine

NRELs offshore 5 MW baseline wind turbine was chosen for this study [47]. Its onshore mode can also be activated. Therefore, offshore and onshore areas can be evaluated globally. Table 2 shows the main characteristics of the turbine.

The power curve between the cut-in and cut-out wind speeds in this study has a data resolution of 0.5 m/s. In the following section, we explain how this power curve is implemented on the wind speed distribution at every ERA5 grid point to obtain the seasonal energy production variations.

2.2. Methodology

2.2.1. Air density and wind speed at hub height

The results shown in this paper are computed to understand the effects of variability in air density on *WPD* and consequent changes in the *SEP* of the turbine. Since we referred to pressure at the surface of the model for the computation of air density, the height up to the model's topography has already been corrected. Only the differences in height between the model and the actual surface must be taken into account. Thus, any correction factor due to

Table 2
Main characteristics of the NREL 5 MW baseline wind turbine.

Rating	5 MW
Rotor Orientation, Configuration	Upwind, 3 Blades
Control	Variable Speed, Collective Pitch
Rotor, Hub Diameter	126 m, 3 m
Hub Height	90 m
Cut-In, Rated, Cut-Out Wind Speed	3 m/s, 11.4 m/s, 25 m/s
Rated Tip Speed	80 m/s

altitude applied to the seasonal air density, wind speed, and therefore WPD, should be applied to the mean values of these parameters in the divider of the ratio.

Furthermore, if the standard atmospheric model is used [48] to compute the air density at 90 m above the surface (the height corresponding to the hub), the reduction with altitude with respect to zero level exceeds 0.99. This deviation is also negligible for the reduction in wind speed according to the log law of the wind shear from 100 m (ERA5's U100 and V100) to 90 m; in the worst case, for a very rough terrain, $log(90/z_0)/log(100/z_0)$ equals 0.96 ($z_0 = 3$ m for "centres of cities with tall buildings" [48]). In the sea, ($z_0 \approx 0.0005$ m), this factor exceeds 0.99. However, as mentioned above, these small correction factors at each grid point should be applied for the absolute values and the relative changes due to air density variations remain almost the same as per the objective of this paper.

2.2.2. Wind power density calculation

As wind power is proportional to both air density and the cube of wind speed, we used the virtual temperature (T_v, in K) and surface pressure (p, in Pa) of ERA5 to obtain density ρ of air (in kg/m^3).

$$\rho = \frac{p}{R' T_v} \tag{4}$$

where $R' = 287.058 J/kg \cdot K$ is the gas constant corresponding to dry air. The computed air density is accurate since via the virtual temperature [49,50].

$$T_v = \left[1 + \left(\frac{1}{\varepsilon} - 1\right) q\right] T = \frac{T}{1 - (1 - \varepsilon)\frac{e}{p}}, \tag{5}$$

with $\varepsilon = \frac{R_v}{R_d} \approx 0.622$, where T denotes the temperature, q refers to specific humidity (kg/kg), and e is the partial pressure of water vapour (Pa). Thus, the changes in density due to humidity are already considered.

Hence, we can finally define the mean *WPD* according to air density and wind speed in the time series of $N_s = 3 \times 10$ monthly cases in 10 years grouped in 3-month long seasons (winter, spring, summer, and autumn) with $i \varepsilon \{1, \ldots, N_s\}$.

$$WPD = \frac{1}{N_s} \sum_{i=1}^{N_s} \frac{1}{2} \rho_i U_i^3, \tag{6}$$

Similarly, the long-term mean air density, or the annual mean air density, for $N_a = 12 \times 10$ cases is

$$\overline{\rho_a} = \frac{1}{N_a} \sum_{i=1}^{N_a} \rho_i \tag{7}$$

Thus, $\overline{\rho_a}$ refers to the reference air density for each ERA5 grid point of the planet, with respect to which the seasonal *WPD* and capacity factor deviations will be computed. First, the global spatial behaviour of the relative change in air density (in percent) in each season is computed.

$$\Delta\rho = \left(\frac{\overline{\rho_s}}{\overline{\rho_a}} - 1\right) \times 100,$$

with $\overline{\rho_s}$ being the air density series of the given season, namely, JFM (winter), AMJ (spring), JAS (summer), and OND (autumn).

Similarly, to compute changes in wind power due to air density variations in a given season, we defined WPD_r, that is, the relative change in wind power density (in percent) between the *WPD* that considers the density variations and the *WPD* that neglects them.

$$\Delta WPD = \left(\frac{\sum_{i=1}^{N_s} \rho_i U_i^3}{\overline{\rho_a} \sum_{i=1}^{N_s} U_i^3} - 1\right) \times 100 \tag{8}$$

where $\overline{\rho_a}$, as mentioned previously, is the reference air density given by the annual average at the site. This methodology allows measurement of seasonal errors in wind power due to air density around the values obtained for a constant air density referenced as the average of the location. These variations are expected to be stronger at the middle and high latitudes of the planet for winter and summer because the influences of temperature on air density (colder air over land areas during winter) and pressure (often, high-pressure areas develop over land regions during winter) are stronger in these areas. Note that the standard reference air density ρ_0 of normalization (Eq. (2)) is expressed as $\overline{\rho_a}$ in this study, that is, the annual average of each location defined in Eq. (7).

2.2.3. Changes in seasonal energy production

To construct the histograms of normalized wind speed, the separated time series of each season were computed with an interval of 0.5 m/s from 0 to 40 m/s. The same interval was used in the power curve of our turbine. Thus, wind statistics can be implemented in the power curve to obtain *SEP*.

The number of cases in each interval was computed as a discrete probability density f_i given by the histogram that fulfils $\sum_{i=1}^{80} f_i = 1$), in which i denotes each interval and P_i is the mean power at that interval i in MW.

$$SEP(TWh) = \sum_{i=1}^{80} (f_i P_i) \cdot (365.25/4) \cdot 24 \cdot 10^{-6} \tag{9}$$

The same procedure was used to compute the non-normalized seasonal production (SEP_n) with the corresponding wind speed histogram and probability density. Thus, the change in the estimation of *SEP* by neglecting the varying density (in percent) was calculated with respect to this value at each location.

$$\Delta SEP = (SEP/SEP_n - 1) \times 100 \tag{10}$$

Additionally, equation (9) was used for the computation of *AEP* for 365.25·24 h and the corresponding discrete probability density. The objective was to remove the grid points that show low capacity factors for our 5 MW (= 5000 kW) turbine (i.e., below 15%). Thus,

$$\frac{AEP}{5000 \cdot 365.25 \cdot 24} < 0.15 \tag{11}$$

Thus, the locations with low winds and energy potential according to typical productive capacity factor limits of the wind industry were omitted in the maps, and only relevant locations are shown [51].

2.2.4. Global spatial averages from gridded fields

Since ERA5 data are given in a regular longitude-latitude grid, global averages of a two-dimensional field z defined over the sphere (any of the magnitudes above) were computed considering the varying areas $A_{i,j}$ corresponding to a grid cell as follows.

$$A_{i,j} = R^2 \int_{\lambda_i - \frac{\Delta\lambda}{2}}^{\lambda_i + \frac{\Delta\lambda}{2}} d\lambda \int_{\theta_j - \frac{\Delta\theta}{2}}^{\theta_j + \frac{\Delta\theta}{2}} \cos\theta d\theta = R^2 \Delta\lambda \sin\left(\frac{\Delta\theta}{2}\right) \cos\theta_j. \tag{12}$$

where R is Earth's radius, λ refers to the longitude, and θ is the latitude. $\Delta\lambda$ and $\Delta\theta$ are the longitude and latitude spacings respectively in the longitude-latitude grid. Using the size of every

grid cell (as seen above), the spatial average of the two-dimensional field z was computed as

$$\overline{z} = \frac{\sum_{i,j} z_{i,j} A_{i,j}}{\sum_{i,j} A_{i,j}}. \quad (13)$$

2.2.5. Analysis of a particular case using the aeroelastic code FAST

A short-term power production analysis was also analysed for high air density (around the first quartile at a relevant location such as Hudson Bay) and low air density (around the third quartile at that location) using the NREL's code FAST [52] implemented on the abovementioned 5 MW turbine. This code presents the options for floating or bottom-fixed offshore and onshore turbines, and its results have been validated in various recent studies [53–55].

This high-low air density comparison was performed for four paradigmatic referential wind speeds: three below the rated wind speed and the last at the rated power. First, turbulent signals were created around these referential wind values on a grid over the rotor plane of the turbine. These turbulent winds served as the inputs of the simulations which were run in a 100 s time series, changing the air density in the aerodynamic package of the simulator with an active pitch control. Although the time evolution of several aeroelastic parameters can be obtained, only the evolution of the instantaneous power was studied for the two extreme air densities at each wind speed. The objective was to obtain a qualitative idea about the behaviour of power difference due to the consideration of high and low air densities below and above the rated power.

3. Results

3.1. Air density error maps

Fig. 1 shows the relative changes in air density during the different seasons at a global scale. It can be noted that the highest increase in air density appears over northern extratropical continental areas during cold seasons. This is particularly relevant for continental regions over North America and Eurasia, particularly during winter (January, February, and March), and to a lesser extent during autumn (October, November, and December). Conversely, land in the same areas recorded values corresponding to the most negative changes in air density during warm seasons over these regions, that is, spring (April, May, and June) and summer (July, August, and September). These results are consistent with a global seasonal cycle which presents high pressures over these land areas during cold seasons, together with low temperatures. These factors combine to produce a higher density over these regions. Conversely, during warmer seasons in the Northern Hemisphere, the effect reverses due to these land areas being warmer and affected by lower pressures, leading to negative relative densities during spring and summer.

Since land masses are much larger over the Northern Hemisphere than over the southern areas at the extratropical latitudes, this signal is most important over the extratropical areas in the Northern Hemisphere. In the Southern Hemisphere, the effect is typically weaker, particularly in the extratropical regions, with important relative changes in density observed only over the southernmost tip of South America, Australia, and parts of Africa, besides Antarctica. The prevalence of the Northern Hemisphere is

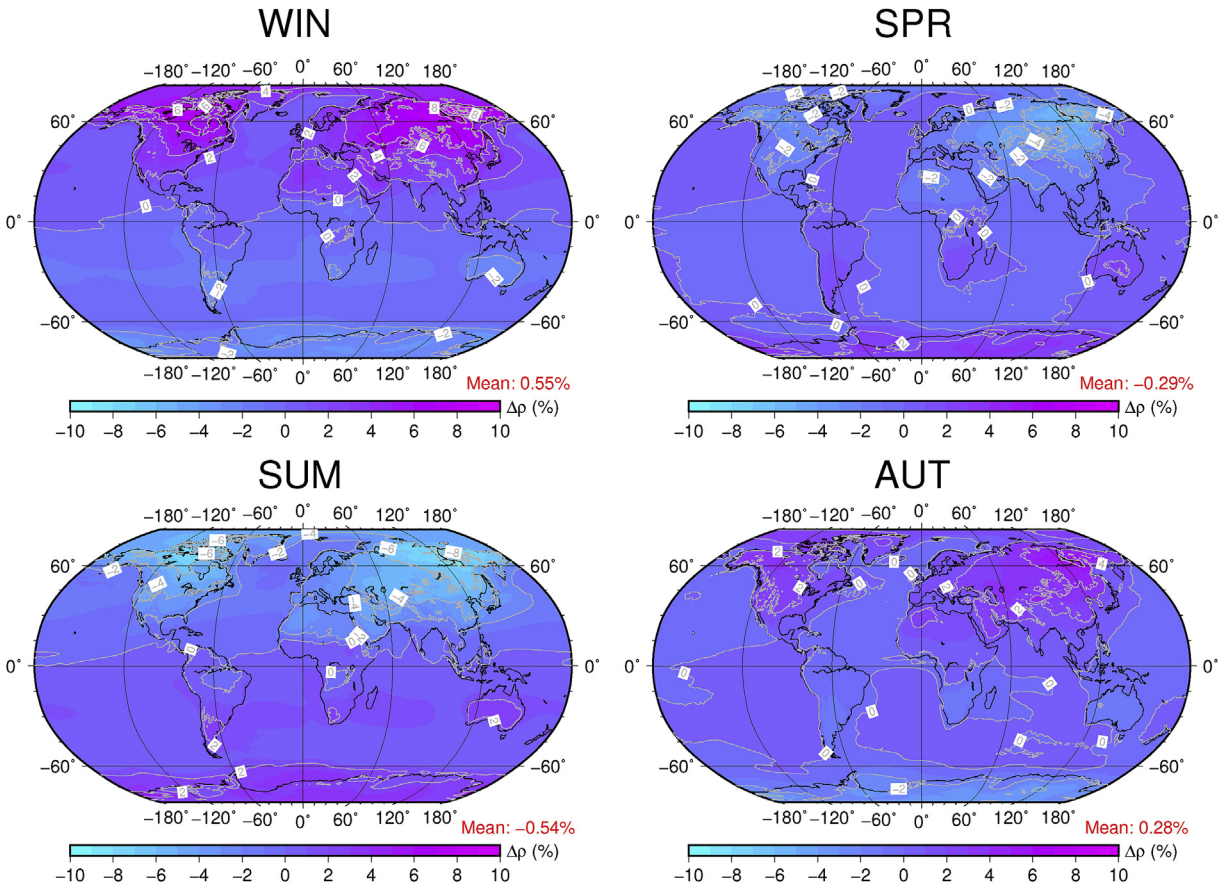

Fig. 1. Changes in air density (in percent) against reference air density in the four seasons.

clear when the globally averaged change in air density is computed (shown in red in Fig. 1). The global means (Eq. (13)) are positive during cold months and negative during warm seasons over the extratropical northern regions. Even though the global means are not very large due to the compensation of positive and negative areas in the different hemispheres, local changes of approximately 10% during winter in Eurasia and North America are observed.

3.2. Seasonal changes in wind power density

In order to quantify the impact of air density changes in wind power density, the distribution of the WPD anomalies associated to the changes in air density are shown in Fig. 2. They very closely resemble the ones presented for the density maps (Fig. 1). Theoretically, from Equation (8), the relationship of the changes in air density to those in wind power are expected to be linear unless there exist substantial covariances between the changes in density and wind speed. In order to check this aspect, a linear model was built for all the grid points shown in Fig. 2, using as predictor the changes in air density shown in Fig. 1. With the exception of autumn, the intercept of the linear model is always higher than 0.9, with the linear model explaining more than 98% of the variance. The relationship is slightly weaker for autumn (October, November, and December), with an intercept of 0.87, and the linear model explaining just 97% of the variance. Thus, the influence of wind density covariances in the estimation of WPD is very weak, and the impact of air density can be considered almost independently of wind.

3.3. Seasonal energy production error maps

Fig. 3 shows the SEP anomalies that are expected if density changes are not properly taken into account during the most extreme seasons of the year (summer and winter), identified using Figs. 1 and 2 above. Winter shows the majority of negative values, locally as high as 25% in some isolated grid points, but values of up to 10% are observed over many areas of the Northern Hemisphere. On the other hand, the Southern Hemisphere shows the majority of negative points during January, February, and March. In general, SEP shows quite an irregular distribution due to extremely low WEP in some areas (these grid points are presented as missing data).

The results are reversed during summer in the Northern Hemisphere since negative changes cover most areas of this hemisphere and positive changes are most often observed in the Southern Hemisphere. As in the previous case, the changes in the Northern Hemisphere affect the global mean of this quantity, amounting to a global mean of 0.8% during winter (the same sign as that for the Northern Hemisphere) and −1.5% during summer (again, the same sign as that of the Northern Hemisphere).

These values seem small but they reflect the mean value over the whole planet, with some grid points showing non-negligible values, as shown from a probability density plot constructed to represent this quantity (Fig. 4).

Zonal and seasonal means of the changes in air density, WPD, and SEP (only for winter and summer this third variable) are shown in Fig. 5. It can be seen that the seasonal cycle of density is very closely related at all latitudes with regard to the relative changes in WPD, while the changes in SEP somewhat differ from the other

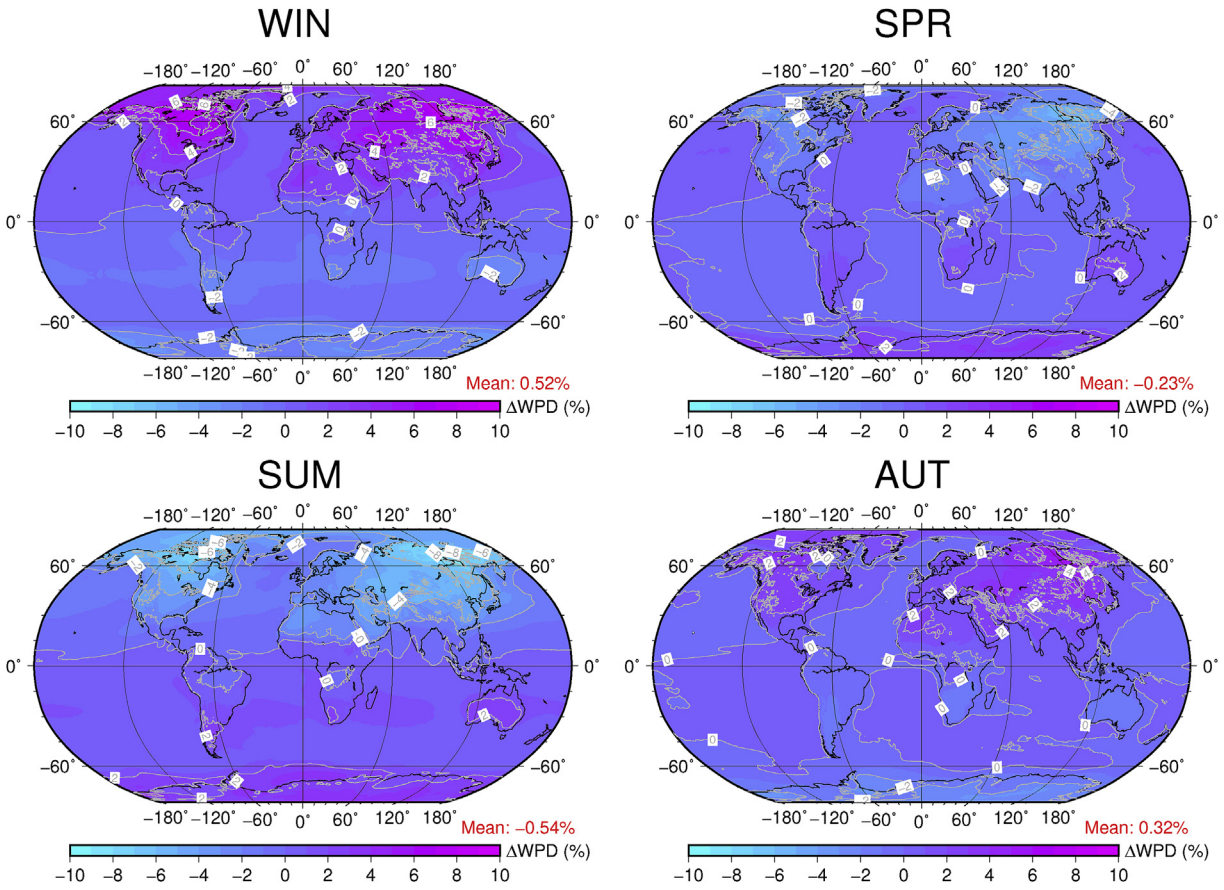

Fig. 2. Global seasonal changes in wind power density (in percent).

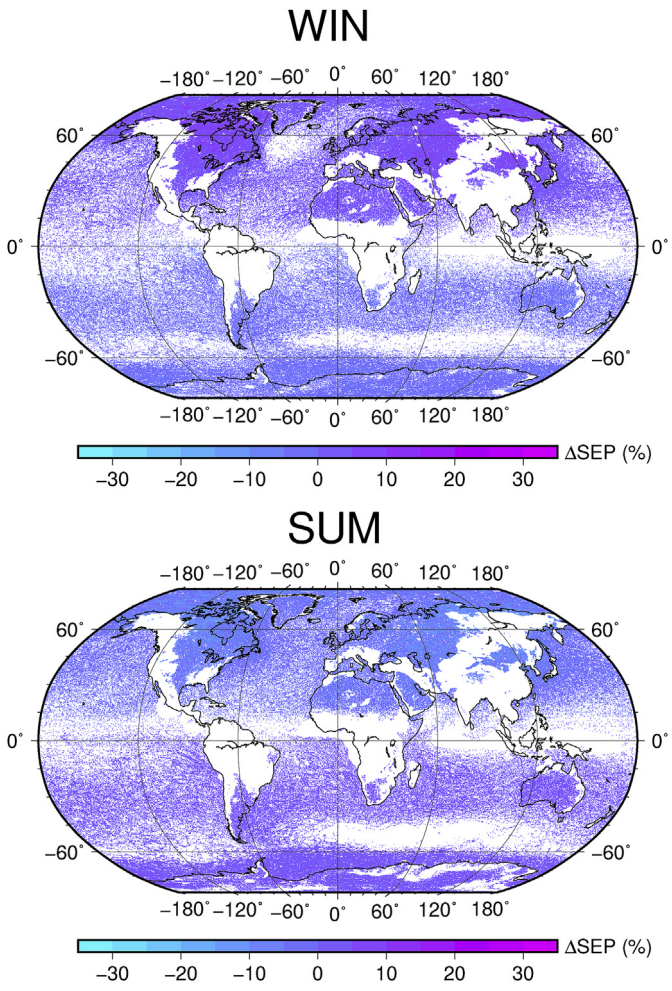

Fig. 3. Global map of winter-to-summer changes (in percent) for Seasonal Energy Production.

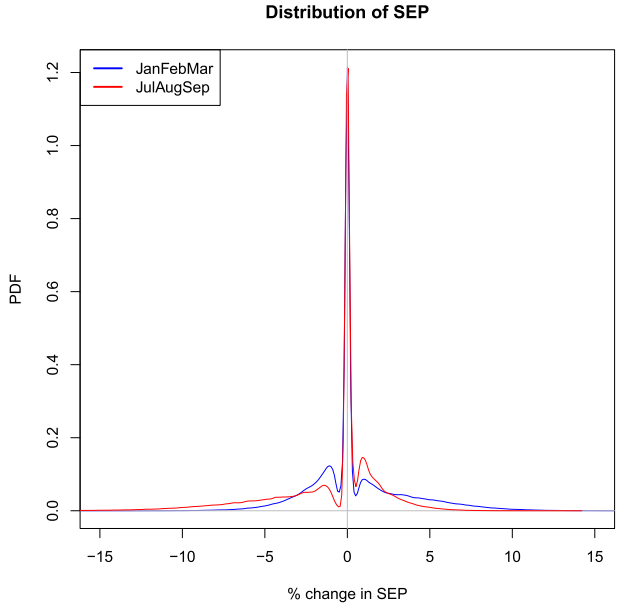

Fig. 4. Probability density function of SEP changes during winter (blue line) and summer (red line) in the Northern Hemisphere. (For interpretation of the references to colour in this figure legend, the reader is referred to the Web version of this article.)

magnitudes, particularly in the extratropical latitudes. The seasonal cycle of wind energy potential and density very closely resembles the (inverted) seasonal cycle of temperature (cold winter in the Northern Hemisphere linked to higher densities, and conversely for the summer in northern months).

Finally, in order to show that the effect can be locally high at particular points, a zoom over the data in Fig. 3 for Hudson Bay is presented in Fig. 6. The area-averaged value over the domain covered by this map is 6% in winter (more energy is estimated when using real densities instead of the average value) and −7% in summer. If particular points are studied, this oscillation can range from −30% to 30%, mainly in the north of the Bay. These are very relevant values from the viewpoint of possible future wind farm implementation in this area because the historical trends of the Hudson Bay, James Bay, and Great Lakes suggest an increasing offshore wind potential while lake ice cover continues to decline [56].

3.4. Simulations with FAST

First, turbulent wind at four referential values was obtained using the package *Turbsim*. The period of simulation was 100 s and the time step was 0.0125 s. The turbulent wind was implemented in the vertical plane of the rotor for a grid with 15 × 15 cells.

Three reference values of wind speed within the U^3 zone of the power curve below the rated power (5, 7.5, and 10 m/s) were used, and the fourth value was a typical value for rated power (15 m/s). These values were chosen because of their paradigmatic behaviour in the instantaneous power time series. In each plot of Fig. 7, the power time series of the high air density (1.3 kg/m^3) appears in red and the power time series corresponding to low air density (1.1 kg/m^3) appears in blue. The value of the air density was changed in the input file *Aerodyn* of FAST. These two interval values of air density were extreme for monthly averages but they are typical values at the 25% and 75% percentiles at middle latitudes for 1-hourly data from ERA5.

Maximum power ratio or *maxPR* is also shown for each wind speed. This parameter measures the maximum difference in percent during the time series between the instantaneous power with high air density and the power with low air density.

As expected, there is no difference at 15 m/s above the rated wind speed since the electric generator establishes the limit of energy production. However, for values below the rated wind speed (5, 7.5, and 10 m/s, corresponding to different intensities of breezes), the difference in the power produced is clearly visualized. The *maxPR* increment for the three cases is 20%, 24%, and 29%. Thus, the fluctuations in air density can create important power production changes below the rated wind speed. This difference increases closer to the rated wind speed. Therefore, it is crucial to note that below the rated power, the energy production of the turbine can be considerably affected due to the presence of high or low air densities. Thus, this effect can lead to severe underestimation or overestimation of the total energy produced by a wind farm throughout the year in some locations.

4. Discussion

Recently, Eurek et al. [26] developed a global wind resource estimation taking into account the changes in air density with the altitude. Although air density is a function of both temperature and pressure, both of which vary by day, season, and geographical location, they used a simple relation between air density and site altitude [57] to obtain the annual average. The present study is an extension of Eurek et al.s work as it considers the correction due to air density for different months of the year, including the effect of

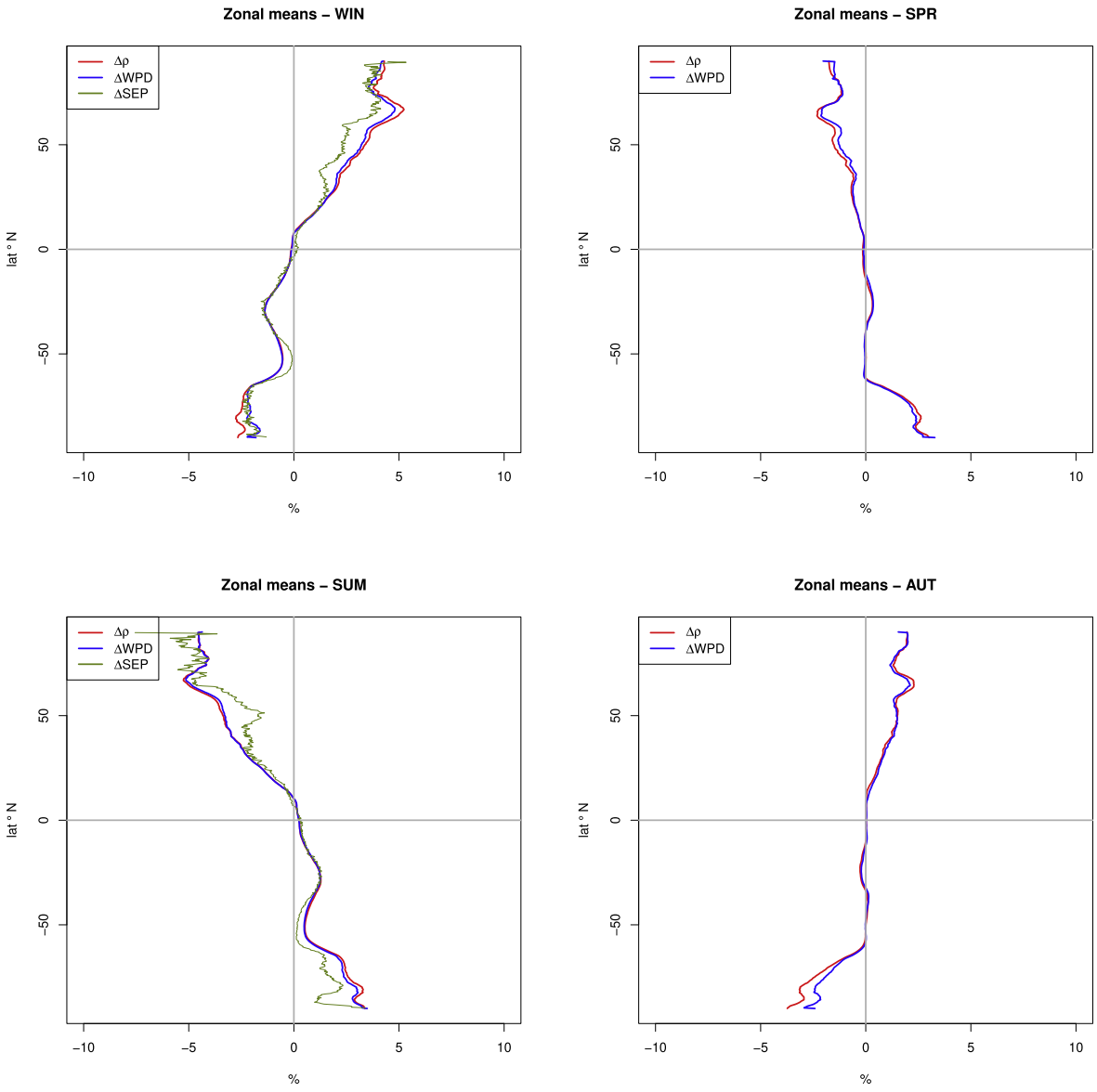

Fig. 5. Global zonal means profiles for $\Delta\rho$, ΔWPD, and.ΔSEP

temperature, pressure, and moisture on air density.

Results regarding both WPD and SEP suggest that the impact of temperature on air density is the most important factor to be considered. This is, to some extent, supported by theoretical considerations. From the equation of the state of moist air (Eq. (4)), considering virtual temperature (Eq. (5)) to include the role of water vapour in the estimation of air density, the relative changes in air density that can be attributed to temperature, pressure, and water vapour pressure can be estimated as follows.

$$\frac{d\rho}{\rho} = \frac{1}{\rho}\frac{\partial\rho}{\partial T}dT + \frac{1}{\rho}\frac{\partial\rho}{\partial P}dP + \frac{1}{\rho}\frac{\partial\rho}{\partial e}de, \tag{14}$$

which can be shown as being equal to

$$\frac{d\rho}{\rho} = -\frac{1}{T}dT + \left(1 + \frac{(1-\varepsilon)e}{P-(1-\varepsilon)e}\right)\frac{dP}{P} - \frac{(1-\varepsilon)}{P-(1-\varepsilon)e}de. \tag{15}$$

The first term, which is associated with changes in temperature, is negative, and basically proportional to the inverse of temperature. This supports the fact that changes in air density reflect the seasonal cycle of temperature with the sign inverted (Fig. 1). The second term is composed of the inverse of pressure multiplied by a term which involves a correction for the partial pressure of water vapour e. Since $e \ll P$, the correction term is negligible and the main effect on air density changes is due to the inverse of pressure (in this case, with the positive sign). Finally, the minus sign in the third term represents the well-known fact that moist air is less dense than dry air. However, since $e \ll P$, this term will also be smaller than the other two terms. The relative values of these terms were computed by the regression of changes in air density with the seasonal means of surface pressure, temperature, and water vapour pressure. The results support that the main factor to be considered while computing the variability in air density is temperature, with a regression coefficient of approximately −0.1%/K for different seasons. Conversely, for surface pressure, the regression coefficient

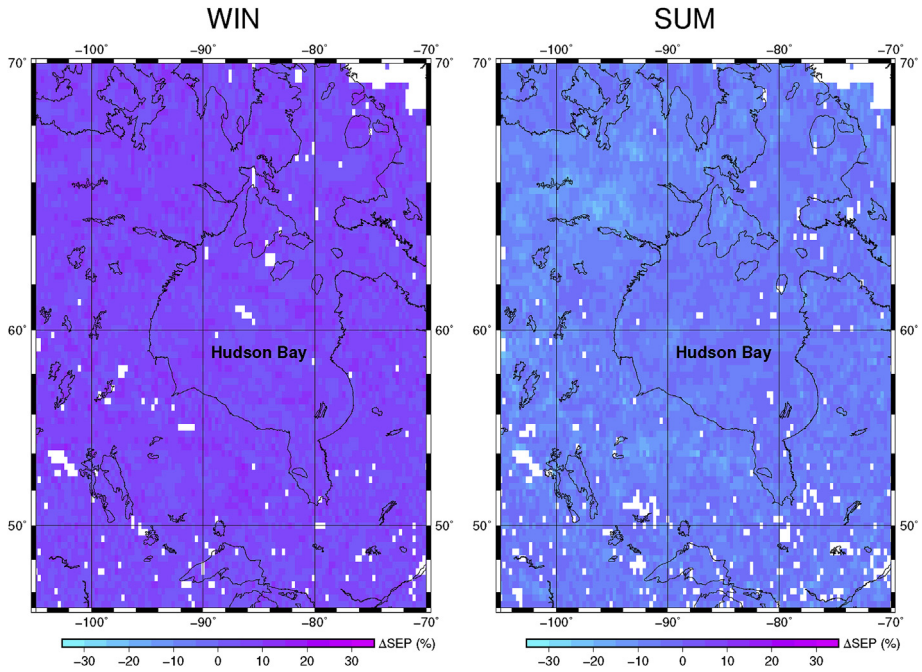

Fig. 6. Percent changes in Seasonal Energy Production at Hudson Bay in winter and summer.

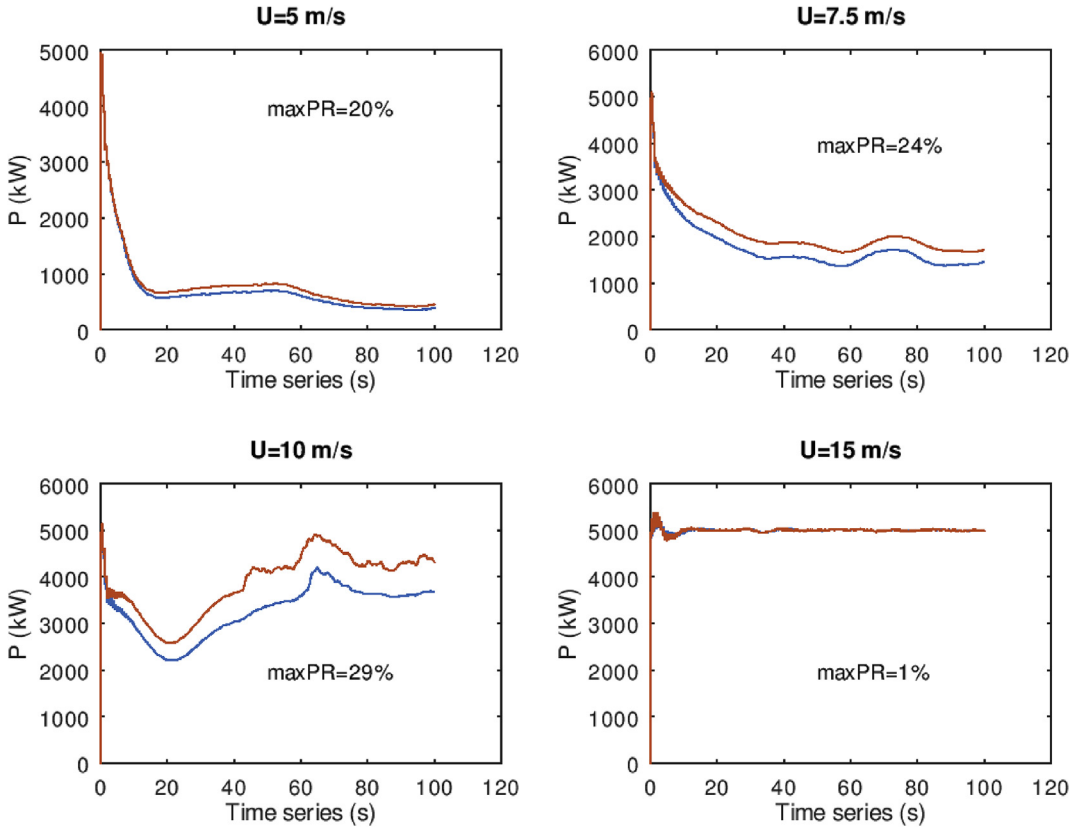

Fig. 7. Simulations using FAST for four characteristic turbulent wind speeds. Red colour: high air density (1.3 kg/m^3). Blue colour: low air density (1.1 kg/m^3). The maximum power ratio (in percent) of the time series (*maxPR*) is shown for each case. (For interpretation of the references to colour in this figure legend, the reader is referred to the Web version of this article.)

ranges from 0.5×10^{-5} to 1×10^{-4} %/Pa, with the highest value being observed during winter and the lowest during summer and spring. This points to the fact that the relative variability in pressure is smaller than the one in temperature and, as such, the effect is weaker. However, we must consider that in some cases, the effects due to pressure and temperature produce the same sign of change. This is particularly true over extratropical land regions during the cold seasons. Over Eurasia and North America in winter, pressures

tend to be higher and temperatures lower during cold seasons. This produces the largest changes in air density. The reverse effect occurs during warm seasons, with summer periods characterized mostly by lower pressures and higher temperatures, leading to smaller densities over summer continental regions. This effect is particularly important over the Northern Hemisphere, characterized by a larger coverage of extratropical continental areas than in the Southern Hemisphere. In the case of moisture, the regression coefficient ranges from small negative values of -1.5×10^{-4} %/Pa to -5×10^{-4} %/Pa during cold seasons, to higher and positive values 1.2×10^{-3} %/Pa to 1.7×10^{-3} %/Pa for spring and summer. In any case, since the variability in water vapour pressure is smaller, the effect is typically weaker than the one associated to temperature.

In this study, the monthly climatological values of surface pressure, temperature, and moisture are used to derive the varying air densities at the global scale. However, one must consider that at extratropical latitudes particularly, transient synoptic-scale systems are very common [27,28]. These extratropical transient systems are characterized by areas of low pressure and meridional transports of warm air. The impact of sub-monthly variability at a global scale with a high-resolution dataset such as the ERA5 reanalysis is a very time-consuming task but would, no doubt, contribute substantially to the literature.

In economic terms, the observed extreme oscillation of 30% in SEP over some points of Hudson Bay implies a deviation of 1 GWh in energy production (Eq. (11)) which corresponds to profits of US $ 100,000 each winter in terms of the cost of energy for offshore wind energy [58], assuming a typical capacity factor of 30% for winter. This is not the selling price, which can be 20% higher without value added tax, and being offshore, it presents the most important case for wind energy. In any case, given the thermoregulatory character of the seas, the most significant variations were found onshore, and they should be studied locally using high-resolution meteorological models that can represent topography with better resolution.

5. Conclusions

In this study, monthly varying surface pressure, temperature, and moisture are considered to evaluate the monthly changes in air density over the average air density at every grid point of ERA5 reanalysis. The changes in air density are primarily due to the changes in temperature, and pressure and moisture exert a lower influence. The changes in air density are most important over extratropical continental areas in which cold seasons are characterized by high pressure systems and lower temperatures. Since the land coverage is higher over the Northern Hemisphere, the global mean change reflects the behaviour in the Northern Hemisphere.

Using these changes in air density, after computing normalized wind speeds, the changes in WPD are computed at every grid point. It can be shown that the covariances between density changes and wind speed changes are very low, and the changes in wind power density are basically due to the changes in air density.

Local factors are very important. The impact of the changes in air density is smaller over tropical areas. Thus, this effect should be analysed in detail using in-situ data or high-resolution numerical model simulations during the detailed planning of new wind farms.

The simulations performed using the aeroelastic code FAST demonstrate the need for these detailed studies, including those regarding the influence of air density changes over short periods of time. The introduction of realistic turbulent winds as inputs in the U^3 zone of the power curve at different air densities clarifies the difference in instantaneous power readings. Further research on this topic may shed light on other possibly important factors affecting other turbines and locations with strong daily thermal oscillations.

Acknowledgments

This work was funded by the Spanish Government's MINECO project CGL2016-76561-R (AEI/FEDER EU) and the University of the Basque Country (UPV/EHU-funded project GIU17/02). The ECMWF ERA-5 data used in this study were obtained from the Copernicus Climate Data Store. All the calculations were carried out in the framework of R Core Team (2016). More can be learnt about R, a language and an environment for statistical computing, at the website of the R Foundation for Statistical Computing, Vienna, Austria (https://www.R-project.org/).

References

[1] Pourrajabian A, Mirzaei M, Ebrahimi R, Wood D. Effect of air density on the performance of a small wind turbine blade: a case study in Iran. J Wind Eng Ind Aerodyn 2014;126:1–10.
[2] Soraperra G. Design of wind turbines for non-standard air density. Wind Eng 2005;29(2):115–28.
[3] Monteiro C, Bessa R, Miranda V, Botterud A, Wang J, Conzelmann G, et al. Wind power forecasting: state-of-the-art 2009. Tech. rep. Argonne National Laboratory (ANL); 2009.
[4] Weisser D. A wind energy analysis of Grenada: an estimation using the Weibull density function. Renew Energy 2003;28(11):1803–12.
[5] Gökçek M, Bayülken A, Bekdemir Ş. Investigation of wind characteristics and wind energy potential in Kirklareli, Turkey. Renew Energy 2007;32(10):1739–52.
[6] Dvorak MJ, Archer CL, Jacobson MZ. California offshore wind energy potential. Renew Energy 2010;35(6):1244–54.
[7] Gross MS, Magar V. Offshore wind energy potential estimation using UPSCALE climate data. Energy Sci Eng 2015;3(4):342–59.
[8] Akdağ SA, Güler Ö. Evaluation of wind energy investment interest and electricity generation cost analysis for Turkey. Appl Energy 2010;87(8):2574–80.
[9] Fueyo N, Sanz Y, Rodrigues M, Montañés C, Dopazo C. High resolution modelling of the on-shore technical wind energy potential in Spain. Wind Energy 2010;13(8):717–26.
[10] Hasager CB, Barthelmie RJ, Christiansen MB, Nielsen M, Pryor S. Quantifying offshore wind resources from satellite wind maps: study area the North Sea. Wind Energy 2006;9(1–2):63–74.
[11] Doubrawa P, Barthelmie RJ, Pryor SC, Hasager CB, Badger M, Karagali I. Satellite winds as a tool for offshore wind resource assessment: the Great Lakes Wind Atlas. Remote Sens Environ 2015;168:349–59.
[12] Carvalho D, Rocha A, Santos CS, Pereira R. Wind resource modelling in complex terrain using different mesoscale–microscale coupling techniques. Appl Energy 2013;108:493–504.
[13] Carvalho D, Rocha A, Gómez-Gesteira M, Santos C. A sensitivity study of the WRF model in wind simulation for an area of high wind energy. Environ Model Softw 2012;33:23–34.
[14] Carvalho D, Rocha A, Gómez-Gesteira M, Santos CS. Sensitivity of the WRF model wind simulation and wind energy production estimates to planetary boundary layer parameterizations for onshore and offshore areas in the Iberian Peninsula. Appl Energy 2014;135:234–46.
[15] Carvalho D, Rocha A, Gómez-Gesteira M, Santos CS. Comparison of reanalyzed, analyzed, satellite-retrieved and NWP modelled winds with buoy data along the Iberian Peninsula coast. Remote Sens Environ 2014;152:480–92.
[16] Carvalho D, Rocha A, Gómez-Gesteira M, Santos CS. WRF wind simulation and wind energy production estimates forced by different reanalyses: comparison with observed data for Portugal. Appl Energy 2014;117:116–26.
[17] Carvalho D, Rocha A, Gómez-Gesteira M, Santos CS. Offshore wind energy resource simulation forced by different reanalyses: comparison with observed data in the Iberian Peninsula. Appl Energy 2014;134:57–64.
[18] Statoil company. 2016-11-20. Tech. rep, https://www.statoil.com/en/news/hywindscotland.html; 2016.
[19] Esteban M, Leary D. Current developments and future prospects of offshore wind and ocean energy. Appl Energy 2012;90(1):128–36.
[20] Gaudiosi G. Offshore wind energy in the world context. Renew Energy 1996;9(1):899–904.
[21] Farkas Z. Considering air density in wind power production. arXiv preprint arXiv:1103.2198.
[22] Collins J, Parkes J, Tindal A. Short term forecasting for utility-scale wind farms. The power model challenge. Wind Eng 2009;33(3):247–57.
[23] Dahmouni A, Salah MB, Askri F, Kerkeni C, Nasrallah SB. Assessment of wind energy potential and optimal electricity generation in Borj-Cedria, Tunisia. Renew Sustain Energy Rev 2011;15(1):815–20.
[24] Svenningsen L. Power curve air density correction and other power curve options in windpro. Tech. rep., Technical report. EMD International A/S; 2010. 2010, www.emd.dk/files/windpro/WindPRO_Power_Curve_Options. pdf.
[25] Yamaguchi A, Ishihara T. Assessment of offshore wind energy potential using

mesoscale model and geographic information system. Renew Energy 2014;69:506–15.
[26] Eurek K, Sullivan P, Gleason M, Hettinger D, Heimiller D, Lopez A. An improved global wind resource estimate for integrated assessment models. Energy Econ 2017;64:552–67.
[27] Grotjahn R. Global atmospheric circulations: observations and theories. Oxford University Press; 1993.
[28] James IN. Introduction to circulating atmospheres. Cambridge, UK: Cambridge University Press; 1994.
[29] Ulazia A, Sáenz J, Ibarra-Berastegui G. Sensitivity to the use of 3DVAR data assimilation in a mesoscale model for estimating offshore wind energy potential. A case study of the Iberian northern coastline. Appl Energy 2016;180:617–27.
[30] A. Ulazia, J. Sáenz, G. Ibarra-Berastegui, S. J. González-Rojí, S. Carreno-Madinabeitia, Using 3DVAR data assimilation to measure offshore wind energy potential at different turbine heights in the West Mediterranean, Applied Energy.
[31] Floors R, Nielsen M. Estimating air density using observations and re-analysis outputs for wind energy purposes. Energies 2019;12(11):2038.
[32] Hansen J, Ruedy R, Glascoe J, Sato M. Giss analysis of surface temperature change. J Geophys Res: Atmosphere 1999;104(D24):30997–1022.
[33] M. Macias Fauria, E. A. Johnson, Large-scale climatic patterns control large lightning fire occurrence in Canada and Alaska forest regions, J Geophys Res: Biogeosciences 111 (G4).
[34] Walsh JE, Mostek A. A quantitative analysis of meteorological anomaly patterns over the United States, 19001977. Mon Weather Rev 1980;108(5):615–30. https://doi.org/10.1175/1520-0493(1980)108¡0615:AQAOMA¿2.0.CO;2.
[35] Hersbach H. The era5 atmospheric reanalysis. In: AGU fall meeting abstracts; 2016.
[36] Dee DP, Uppala SM, Simmons AJ, Berrisford P, Poli P, Kobayashi S, Andrae U, Balmaseda MA, Balsamo G, Bauer P, Bechtold P, Beljaars ACM, van de Berg L, Bidlot J, Bormann N, Delsol C, Dragani R, Fuentes M, Geer AJ, Haimberger L, Healy SB, Hersbach H, Hlm EV, Isaksen L, Kllberg P, Khler M, Matricardi M, McNally AP, Monge-Sanz BM, Morcrette J-J, Park B-K, Peubey C, de Rosnay P, Tavolato C, Thpaut J-N, Vitart F. The ERA-Interim reanalysis: configuration and performance of the data assimilation system. Q J R Meteorol Soc 2011;137(656):553–97.
[37] Ulazia A, Gonzalez-Rojí SJ, Ibarra-Berastegi G, Carreno-Madinabeitia S, Sáenz J, Nafarrate A. Seasonal air density variations over the east of scotland and the consequences for offshore wind energy. In: 2018 7th international conference on renewable energy research and applications (ICRERA), IEEE; 2018. p. 261–5.
[38] Rabanal A, Ulazia A, Ibarra-Berastegi G, Sáenz J, Elosegui U. Midas: a benchmarking multi-criteria method for the identification of defective anemometers in wind farms. Energies 2019;12(1):28.
[39] Olauson J. Era5: the new champion of wind power modelling? Renew Energy 2018;126:322–31.
[40] Aniskevich S, Bezrukovs V, Zandovskis U, Bezrukovs D. Modelling the spatial distribution of wind energy resources in Latvia. Latv J Phys Tech Sci 2017;54(6):10–20.
[41] Sterl S, Liersch S, Koch H, van Lipzig NP, Thiery W. A new approach for assessing synergies of solar and wind power: implications for west africa. Environ Res Lett 2018;13(9):094009.
[42] Camargo LR, Gruber K, Nitsch F. Assessing variables of regional reanalysis data sets relevant for modelling small-scale renewable energy systems. Renew Energy 2019;133:1468–78.
[43] Hörsch J. Pypsa-eur: an open optimization model of the european transmission system (dataset). https://github.com/FRESNA/pypsa-eur; 2017.
[44] Allaerts D, Broucke SV, van Lipzig N, Meyers J. Annual impact of wind-farm gravity waves on the belgian–Dutch offshore wind-farm cluster. In: Journal of physics: conference series, vol. 1037. IOP Publishing; 2018. p. 072006.
[45] P. Bechtle, M. Schelbergen, R. Schmehl, U. Zillmann, S. Watson, Airborne wind energy resource analysis, Renew Energy.
[46] Engelhorn T, Müsgens F. How to estimate wind-turbine infeed with incomplete stock data: a general framework with an application to turbine-specific market values in Germany. Energy Econ 2018;72:542–57.
[47] J. Jonkman, S. Butterfield, W. Musial, G. Scott, reportDefinition of a 5-mw reference wind turbine for offshore system development, National Renewable Energy Laboratory, Golden, CO, Technical Report No. NREL/TP-500-38060.
[48] Manwell JF, McGowan JG, Rogers AL. Wind energy explained: theory, design and application. John Wiley & Sons; 2010.
[49] Bohren CF, Albrecht BA. Atmospheric thermodynamics. New York, USA: Oxford University Press; 1998.
[50] Petty GW. A first course in atmospheric thermodynamics. Madison, WI, USA: Sundog Publishers; 2008.
[51] Boccard N. Capacity factor of wind power realized values vs. estimates. Energy Policy 2009;37(7):2679–88. URL, https://doi.org/10.1016/j.enpol.2009.02.046. http://www.sciencedirect.com/science/article/pii/S030142150900144X.
[52] NWTC information portal (FAST). last modified 04-january-2018 ; accessed 10-march-2019, Tech. rep, https://nwtc.nrel.gov/FAST; 2019.
[53] Kecskemety KM, McNamara JJ. Influence of wake dynamics on the performance and aeroelasticity of wind turbines. Renew Energy 2016;88:333–45.
[54] S. Guntur, J. Jonkman, R. Sievers, M. A. Sprague, S. Schreck, Q. Wang, A validation and code-to-code verification of fast for a megawatt-scale wind turbine with aeroelastically tailored blades, Wind Energy Sci Discuss 2 (NREL/JA-5000-68025).
[55] Guntur S, Jonkman J, Schreck S, Jonkman B, Wang Q, Sprague M, Hind M, Sievers R. Fast v8 verification and validation for a megawatt-scale wind turbine with aeroelastically tailored blades. Tech. rep. Golden, CO (United States): National Renewable Energy Lab.(NREL); 2016.
[56] Ashtine M, Bello R, Higuchi K. Assessment of wind energy potential over ontario and great lakes using the narr data: 19802012. Renew Sustain Energy Rev 2016;56:272–82. URL, https://doi.org/10.1016/j.rser.2015.11.019. http://www.sciencedirect.com/science/article/pii/S136403211501271X.
[57] D. Elliott, C. Holladay, W. Barchet, H. Foote, W. Sandusky, reportWind energy resource atlas of the United States, NASA STI/Recon Technical Report N 87.
[58] Department of energy and climate change (decc). https://www.gov.uk/government/organisations/department-of-energy-climate-change. [Accessed 10 March 2019].